

Suppression of antiferromagnetism by pressure in CaCo_2P_2 R. E. Baumbach,^{1,*} V. A. Sidorov,^{1,2} Xin Lu,^{1,†} N. J. Ghimire,¹ F. Ronning,¹ B. L. Scott,³ D. J. Williams,⁴
E. D. Bauer,¹ and J. D. Thompson¹¹*Materials Physics and Applications, Condensed Matter and Magnet Science, Los Alamos National Laboratory, Los Alamos, New Mexico 87545, USA*²*Institute for High Pressure Physics, Russian Academy of Sciences, 142190 Troitsk, Moscow, Russia*³*Materials Physics and Applications 11, Los Alamos National Laboratory, Los Alamos, New Mexico 87545, USA*⁴*Materials Physics and Applications, Center for Integrated Nanotechnologies, Los Alamos National Laboratory, Los Alamos, New Mexico 87545, USA*

(Received 4 December 2013; revised manuscript received 17 February 2014; published 10 March 2014)

We report magnetization M , heat capacity C , and electrical resistivity ρ for single crystals of the itinerant electron antiferromagnet CaCo_2P_2 ($T_N \approx 110$ K). Measurements at ambient pressure reveal rich magnetic behavior, where ferromagnetic correlations are present in the paramagnetic state and a subsequent feature is seen at $T_1 \approx 22$ K within the ordered state. Heat-capacity measurements additionally reveal moderately enhanced electronic correlations, as evidenced by the electronic coefficient of the specific heat $\gamma = 23$ mJ/mol·K², which is large by comparison to closely related 122 analogs and the value predicted by electronic structure calculations. Upon the application of pressure, T_N is suppressed toward zero. For $P \geq 0.89$ GPa, another phase transition appears at $T_2 < T_N$ which is also suppressed by P . At $P_c \approx 1.4$ – 1.5 GPa, T_N and T_2 drop abruptly to zero at a putative quantum phase transition. For $P > P_c$, a broad shoulder in $\rho(T)$ appears at T^* , which moves to higher T and broadens with increasing P . We discuss possible scenarios to understand the phase diagram and compare to other compounds which show similar P -driven behavior.

DOI: [10.1103/PhysRevB.89.094408](https://doi.org/10.1103/PhysRevB.89.094408)

PACS number(s): 75.30.-m, 74.62.Fj, 73.43.Nq

I. INTRODUCTION

There have been extensive investigations of f -electron compounds where a parameter δ (e.g., pressure P , chemical substitution x , or magnetic field H) tunes a second-order magnetic phase transition to zero temperature, often as a result of the delicate interplay between the Ruderman-Kittel-Kasuya-Yosida interaction and the Kondo effect [1–4]. At the resulting quantum critical point (QCP), emergent phenomena including non-Fermi-liquid behavior and unconventional superconductivity are often observed. These phase diagrams share some similarities with those of the d -electron iron pnictide and cuprate materials, where the high-temperature superconductivity and deviations from Fermi-liquid behavior appear to be related to the spin fluctuations that emerge as the magnetic order is suppressed toward zero [5,6]. Unfortunately, although it is attractive to apply this picture generically, for a variety of reasons many d -electron magnets avoid analogous behavior. For instance, while the magnetism of the stoichiometric compounds MnSi [7–9] and ZrZn₂ [10–12] can be suppressed by P , the phase transition is first order at all P for MnSi and becomes first order near zero temperature for ZrZn₂, owing to the coupling between the fermionic modes and the ferromagnetic critical fluctuations. There additionally are many d -electron systems where chemical substitution tunes the magnetism toward zero, e.g., $(\text{Ni}_{1-x}\text{Pd}_x)_3\text{Al}$ [13] and $\text{Cr}_{1-x}\text{V}_x$ [14]. However, the disadvantage to chemical substitution is that it typically introduces disorder, which

obscures the ground-state behavior and/or destroys superconductivity. Therefore, there remains strong motivation to search for additional d -electron materials where a QCP can be accessed by a clean tuning parameter, such as pressure.

Given the vast number of known d -electron compounds, it is useful to limit a search for quantum criticality by applying some rudimentary arguments. For instance, layered structures can promote interesting behavior since they often favor a two-dimensional Fermi surface, which can enhance electronic correlations and/or provide nesting between different Fermi-surface sheets. The ThCr_2Si_2 -type structure is a well-known example, with over 600 phases [15], many of which exhibit unusual physics including quantum critical behavior (e.g., CePd_2Si_2 [16] and YbRh_2Si_2 [17]) and high-temperature superconductivity (e.g., $M\text{Fe}_2\text{As}_2$, where $M = \text{Ca, Sr, Ba}$) [18]. Although significantly less well studied than their As-based relatives, the phosphorous based $MT_2\text{P}_2$ compounds [19–21] ($T =$ transition metal) and related phases (e.g., $Ln\text{FePO}$, where $Ln = \text{La-Sm}$ [22–24]) also exhibit interesting behavior including complicated interplay between superconductivity, magnetism, and structural instabilities.

A particularly interesting example is CaCo_2P_2 , which crystallizes in the collapsed tetragonal (cT) ThCr_2Si_2 phase (MT_2X_2), wherein the X - X bonding between neighboring T - X layers reduces the interlayer distance and relaxes the in-plane lattice constants, by comparison to the uncollapsed (ucT) phase [25,26]. Such structural variability is of interest, in part, because it modifies the Fermi surface: i.e., while the ucT phase promotes a two-dimensional-like Fermi surface, the cT phase favors three-dimensional behavior [27,28]. Additionally, CaCo_2P_2 exhibits itinerant electron antiferromagnetic ordering at a Néel temperature $T_N \approx 110$ K where the magnetism arises

*Corresponding author: baumbach@magnet.fsu.edu

†Present address: Center for Correlated Matter, Zhejiang University, Hangzhou 310058, China.

from the Co ions, which are arranged ferromagnetically in the a - b plane and antiferromagnetically along the c axis for $T \leq T_N$ [29]. A second characteristic temperature is seen at $T_1 \approx 20$ K, where the magnetic susceptibility decreases with decreasing T . In contrast to the Pauli paramagnets CaFe_2P_2 and CaNi_2P_2 , the magnetism in CaCo_2P_2 is expected to be due to a narrow $3d$ electron band being found near the Fermi energy [30,31]. These observations motivated several recent studies, including investigations of $\text{Sr}_{1-x}\text{Ca}_x\text{Co}_2\text{P}_2$, in which the evolution from ucT for SrCo_2P_2 to cT for CaCo_2P_2 drives an unusual evolution in the magnetic ground state, and $\text{Ca}(\text{Co}_{1-x}\text{T}_x)_2\text{P}_2$ ($T = \text{Fe, Ni}$), where electronic tuning and chemical pressure suppress T_N toward zero temperature [19,32].

Herein, we report results for single crystals of CaCo_2P_2 under applied pressure. We first revisit the zero pressure behavior of the magnetization M , heat capacity C , and electrical resistivity ρ . We show that antiferromagnetic ordering occurs near $T_N \approx 110$ K which is followed by another feature at $T_1 \approx 22$ K. In addition, the magnetic susceptibility for $T > T_N$ reveals ferromagnetic correlations in the paramagnetic state. We also confirm that the electronic coefficient of the heat capacity is moderately large ($\gamma = 23$ mJ/mol·K²) by comparison to (1) related d -electron 122 compounds and (2) the expected value for γ in the unpolarized state predicted by electronic structure calculations. This result suggests the presence of moderate electronic correlations.

After establishing the zero pressure behavior, we explore the influence of applied pressure on the electrical resistivity. Here, we find that T_N is suppressed with increasing P and, for $P \geq 0.89$ GPa, a second phase transition appears at $T_2 < T_N$. For $P_c \approx 1.4$ – 1.5 GPa, T_N drops abruptly to zero at a putative quantum phase transition (QPT), possibly indicating that the transition to the ordered state becomes first order. The low-temperature power-law dependence of the electrical resistivity suggests Fermi-liquid behavior throughout the entire phase diagram. We also find that although the Fermi-liquid coefficient A begins to increase for $P \leq 1.22$ GPa (suggesting quasiparticle mass enhancement) it is cut off before P_c . For $P > P_c$, A relaxes to smaller values with increasing P and a broad shoulder appears at T^* , which moves to higher T and broadens with increasing P .

II. METHODS

Single crystals of CaCo_2P_2 were grown from elements in a molten Sn flux, as reported previously [25]. The crystal structure and chemical composition were verified by means of single-crystal x-ray-diffraction and energy dispersive x-ray (EDX) analysis, where we find the lattice constants $a = 3.8647$ Å and $c = 9.5841$ Å (at 140 K) and the expected molar ratio Ca:Co:P = 1:2:2. Magnetization $M(T, H)$ measurements were carried out for temperatures $T = 1.8$ – 350 K under an applied magnetic field of $H = 1$ kOe and at $T = 2$ K up to $H = 60$ kOe for fields applied both parallel (\parallel) and perpendicular (\perp) to the c axis using a Quantum Design magnetic property measurement system. The specific heat $C(T)$ was measured for $T = 1.8$ – 120 K using a Quantum Design physical property measurement system.

Electrical resistivity measurements for pressures $P \leq 1.52$ GPa were performed using a BeCu/NiCrAl hybrid

clamp-type pressure cell with silicone fluid as the pressure medium, which provides a nearly hydrostatic environment. The pressure at low temperatures was determined from the superconducting resistive transition of Pb. Further electrical resistivity measurements were performed under hydrostatic pressures up to 5.3 GPa. Here, the high-pressure environment was generated using a miniature clamped toroid-type anvil cell [33,34]. The 122 crystal, along with a piece of Pb whose superconducting transition temperature served as a measure of the pressure, was placed in a teflon capsule filled with glycerol-water (3:2 by volume) pressure-transmitting liquid, which solidifies at room temperature near 5.3 GPa. The cell assembly was cooled slowly from room temperature to 1.7 K. The width of the superconducting transition of Pb did not exceed 10 mK at the highest pressure, an indication of good hydrostatic conditions. Four-point resistivity measurements were performed using an SR830 lock-in amplifier, SR554 transformer preamplifier, and a stable ac-current source [35]. The electrical contacts (Pt wire, 25 μm in diameter) were attached using micro spot welding. Three different samples (S1, S2, and S3) were measured during the different experiments in the two pressure cells, all of which revealed nearly identical behaviors.

Electronic structure calculations are performed using the WIEN 2K code [36] under the generalized gradient approximation and employing the exchange correlation potentials of Perdew, Burke, and Ernzerhof [37].

III. RESULTS: $P = 0$

The magnetic susceptibility $\chi(T) = M(T)/H$ data for $H = 1$ kOe applied parallel (\parallel) and perpendicular (\perp) to the c axis are summarized in Fig. 1(a). From 350 K, $\chi(T)$ increases with decreasing T and evolves through a hump near the Néel temperature $T_N = 110$ K, as reported previously [25,29]. Curie-Weiss (CW) behavior given by the expression

$$\chi(T) = C/(T - \Theta) \quad (1)$$

is observed for $200 \leq T \leq 350$ K, where $\Theta = 92$ K (101 K) for $H \parallel (\perp) c$, indicating ferromagnetic correlations with little anisotropy [Fig. 1(b)]. The point of view that ferromagnetic correlations are present for $T > T_N$ is further supported by the behavior of χT [Fig. 1(b)], which is a measure of the Curie constant C modified by $(T - \theta)^{-1}$. When antiferromagnetic correlations are present (i.e., negative θ) or if μ_{eff} decreases with decreasing T (e.g., due to crystalline electric-field splitting of the Hund's rule multiplet), χT will decrease. In contrast, χT increases with decreasing T only when ferromagnetic correlations are present, as is seen in our data. We additionally find that the Curie constants C yield effective magnetic moments $\mu_{\text{eff}} \approx 1.1\mu_B/\text{Co}$ ($1.0\mu_B/\text{Co}$) for $H \parallel (\perp) c$, which are significantly reduced from that of localized Co^{2+} ions ($\mu_{\text{eff}} = 3.87\mu_B/\text{Co}$ for Co^{2+} with orbital quenching). We further point out that neutron-scattering measurements show that the ordered moment $\mu_{\text{ord}} = 0.32\mu_B$, which is roughly one third of μ_{eff} [29]. These results are consistent with the magnetism arising from itinerant Co d electrons. Following its initial increase, χT decreases for $T < T_N$, revealing the onset of antiferromagnetic correlations in the ordered state. Finally, $\chi(T)$ goes through a sharp reduction at

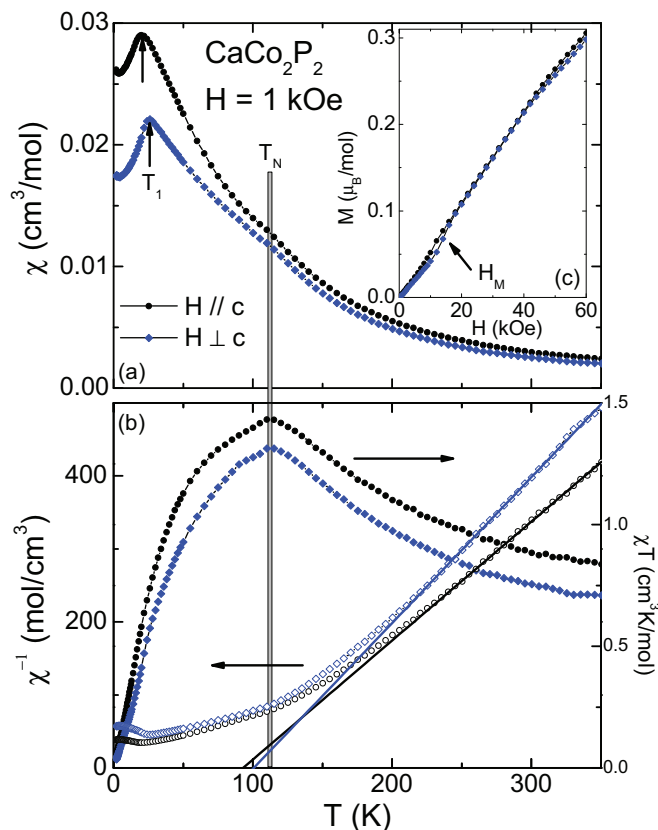


FIG. 1. (Color online) (a) Magnetic susceptibility $\chi(T) = M(T)/H$ data for $H = 1$ kOe applied parallel (\parallel) and perpendicular (\perp) to the c axis. (b) Inverse magnetic susceptibility χ^{-1} and χT vs T . (c) M vs H for $H \parallel$ and $\perp c$ for $T = 2$ K.

a second characteristic temperature $T_1 \approx 22$ K (25 K) for $H \parallel$ (\perp) c . This feature was reported previously by Reehuis *et al.* [29], but was not seen for polycrystalline specimens that were recently investigated [19,32].

In order to further investigate the low-temperature magnetism, we performed magnetization M vs H measurements at $T = 2$ K [Fig. 1(c)]. Here we find that for both field directions the magnetization initially increases linearly with increasing field, as expected for an antiferromagnetically ordered state. For $H \parallel$ (\perp) c , we find evidence for a metamagnetic phase transition near $H_{M,1} = 10$ kOe (12 kOe) where the magnetization abruptly increases. Above H_M the magnetization again increases nearly linearly, with slight negative curvature.

Heat-capacity measurements are shown in Fig. 2(a), where the dominant contribution to C/T is the phonon term. A lambda-like anomaly appears in C/T near $T_N = 108$ K [Fig. 2(b)], in close agreement with our result from $\chi(T)$, with a jump size $\Delta C/T \approx 10$ mJ/mol·K². The shape of the anomaly reveals that the phase transition at T_N is second order. Careful examination of the heat-capacity data does not reveal a jump near $T_1 = 22$ K, although it is possible that if it is subtle it might be hidden by the lattice contribution.

We fit the low-temperature data using the expression $C/T = \gamma + \beta T^2$, where $\gamma = 23$ mJ/mol·K² and $\beta = 0.107$ mJ/mol·K⁴ ($\theta_D \approx 450$ K) are the electronic coefficient of

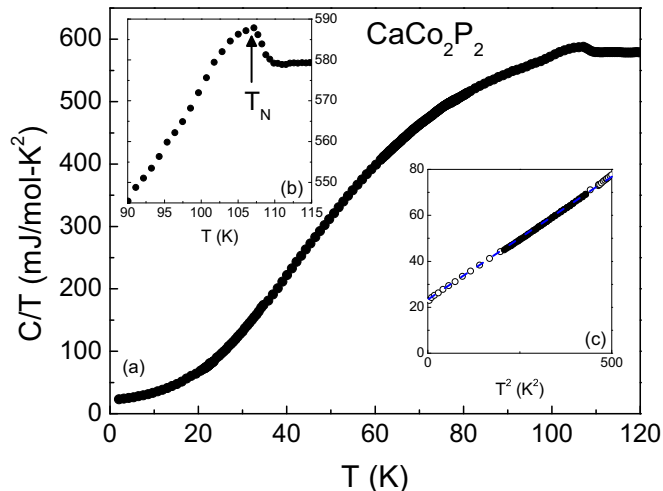


FIG. 2. (Color online) (a) Heat capacity divided by temperature, C/T vs T , for CaCo_2P_2 . (b) C/T in the vicinity of the Néel temperature T_N . (c) C/T vs T^2 at low temperatures. The dotted line that extends to $T = 0$ is a fit to the data using the expression $C/T = \gamma + \beta T^2$, as described in the text.

the heat capacity and the prefactor to the phonon contribution, respectively [Fig. 2(c)]. The value of γ is enhanced by comparison to the related P-based 122 compounds which do not exhibit magnetic ordering (e.g., CaNi_2P_2 and CaFe_2P_2 where $\gamma \approx 5$ and 8 mJ/mol·K², respectively [32]), suggesting the presence of moderate electronic correlations. In order to address this possibility, we show the projected electronic density of states (DOS) for CaCo_2P_2 in Fig. 3, which was calculated in the unpolarized state. We find that there are two sharp peaks in the total DOS near the Fermi energy, which are due to the Co ions. The Fermi energy is located at the minimum between the two peaks, resulting in a calculated electronic coefficient of the specific heat $\gamma = 7.3$ mJ/mol·K². Given that itinerant magnetism should gap parts of the Fermi surface, thereby reducing the electronic specific heat, it is clear that the experimental value of $\gamma = 23$ mJ/mol·K² (which is in the magnetically ordered state) is enhanced by comparison

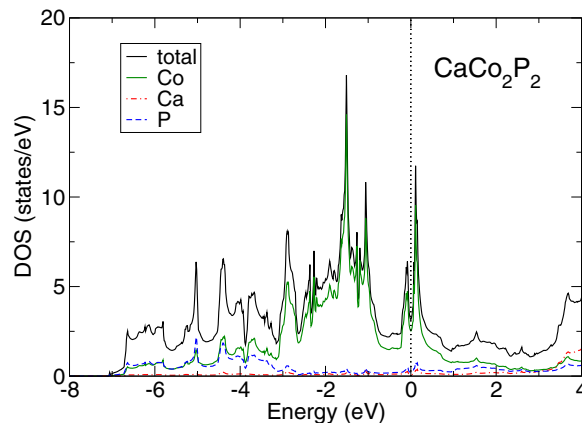


FIG. 3. (Color online) (a) The projected electronic density of states (DOS) for CaCo_2P_2 . Note that the Co atoms contribute the dominant double peak structure near the Fermi energy.

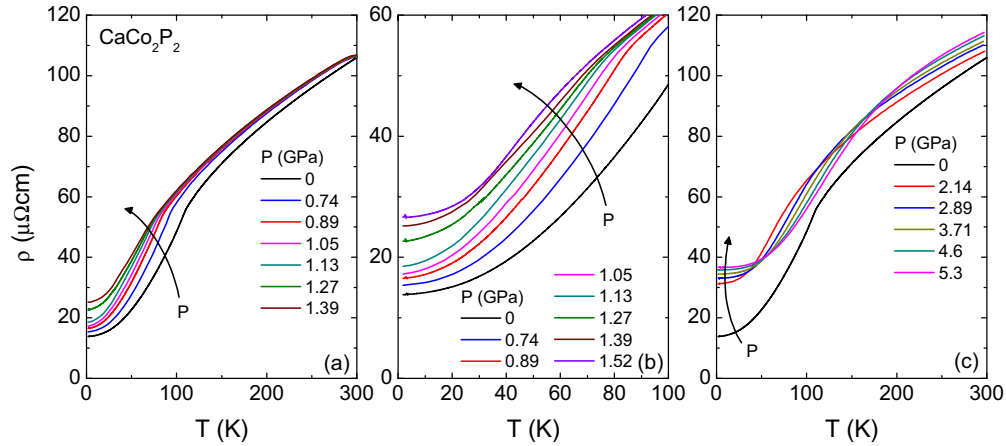


FIG. 4. (Color online) (a) Representative curves of electrical resistivity ρ vs temperature T for CaCo_2P_2 under applied pressure $P \leq 1.39$ GPa. (b) ρ vs T for CaCo_2P_2 for $P \leq 1.52$ GPa, emphasizing the low T region. (c) ρ vs T for CaCo_2P_2 for $P \geq 2.14$ GPa.

to the band calculations. This result suggests the presence of enhanced electronic correlations.

Taken together, the magnetization and heat-capacity data reinforce the notion that CaCo_2P_2 is a moderately correlated itinerant electron antiferromagnet with $T_N \approx 110$ K. Our measurements also emphasize that the magnetism is somewhat complicated. Evidence for this is seen in (1) the presence of ferromagnetic fluctuations for $T > T_N$, (2) the additional feature that is seen at T_1 , and (3) the metamagnetic transition seen in $M(H)$ at H_M . We point out that the earlier neutron-scattering results do not contradict our results regarding T_N and T_1 , as they merely show that there is a component of the magnetic moment of the Co atoms which orders ferromagnetically in the basal plane and antiferromagnetically along the c axis, corresponding to a propagation vector $\mathbf{k} = (0, 0, 1)$. This result does not rule out the possibility that the magnetically ordered state is initially incompletely polarized, i.e., that small perturbations to \mathbf{k} occur with decreasing T at T_1 . In fact, the temperature dependence of the intensity of the magnetic $(001)_M$ peak from neutron-scattering experiments undergoes an increase roughly at T_1 [29]. Further neutron-scattering experiments will be useful to clarify this point.

IV. RESULTS: $P > 0$

Figures 4(a)–4(c) present representative electrical resistivity data for CaCo_2P_2 under applied pressure. Metallic behavior is seen for all P with residual resistivity ratios $\text{RRR} = \rho_{295\text{K}}/\rho_0$ between 4 and 5. At elevated temperatures, $\rho(T)$ exhibits a sublinear temperature dependence for all P , which is anomalous by comparison to the nonmagnetic analog CaNi_2P_2 , where the lattice contribution is dominant over the same temperature range [32].

In the low-pressure region ($P \leq 1.39$ GPa), $\rho(T)$ is abruptly reduced at T_N due to the removal of spin disorder scattering by the antiferromagnetic ordering. T_N appears as a pronounced peak in $\partial\rho/\partial T$ over this pressure range [Fig. 5(a)] that moves to lower T with increasing P at a rate $\partial T_N/\partial P = -33$ K/GPa. This rate of suppression is comparable to what is seen in the analogous iron-arsenide superconductors that crystallize in the ucT ThCr_2Si_2 structure [38]. We also find a broad hump in

$\partial\rho/\partial T$ which moves to lower temperatures and becomes more pronounced with increasing pressure. For ambient pressure, the hump is found roughly between 55 and 65 K [dotted lines, Fig. 5(b)]. At zero pressure, we find no change in $\partial\rho/\partial T$ at $T_1 \approx 22$ K that corresponds to the reduction of $\chi(T)$ at

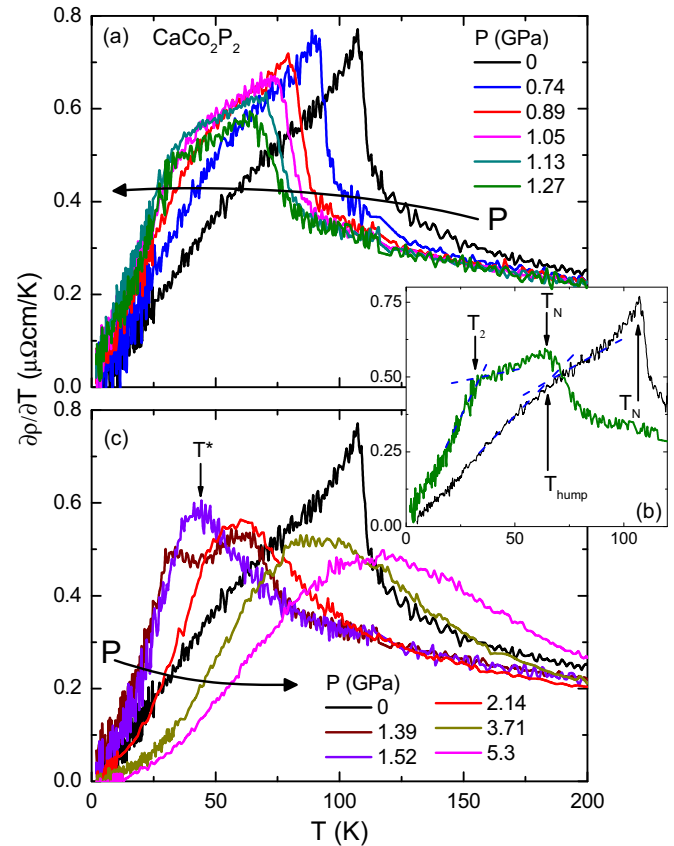


FIG. 5. (Color online) (a) Representative curves of the derivative of the electrical resistivity with respect to temperature $\partial\rho/\partial T$ vs T for $P \leq 1.27$ GPa. The Néel temperature T_N appears as a sharp cusp. (b) $\partial\rho/\partial T$ vs T for $P = 0$ and 1.27 GPa where the criteria that were used to define T_N , T_{hump} , and T_2 are illustrated. (c) $\partial\rho/\partial T$ vs T for $P \geq 1.39$ GPa. T^* appears as a broad hump.

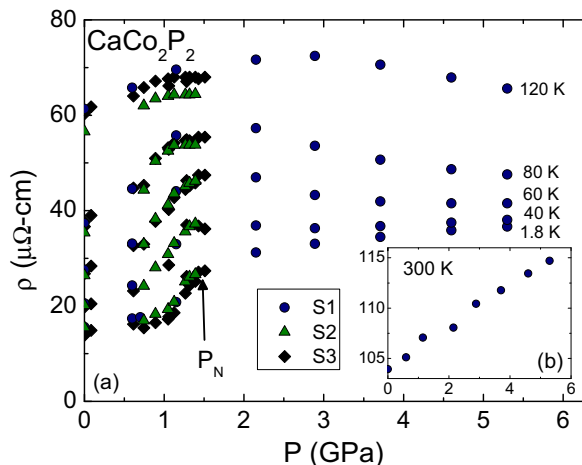


FIG. 6. (Color online) (a) Electrical resistivity ρ vs pressure P at constant temperatures for samples S1, S2, and S3. The Néel temperature appears as a sharp increase at P_N . (b) $\rho(P)$ for $T = 300$ K.

this temperature. Near 0.89 GPa, an additional feature at T_2 emerges and is subsequently suppressed with increasing P [Fig. 5(b)]. For $P > 1.5$ GPa, the double peak structure that is due to T_N and T_2 is replaced by a single hump at T^* , which broadens and moves to higher T with increasing P [Fig. 5(c)].

In order to better understand the behavior for $P = 1.4$ – 1.5 GPa, we consider plots of $\rho(P)$ [Fig. 6(a)] at constant temperature. Data taken for three different samples are shown, revealing a high degree of reproducibility. Here, we find that the resistivity initially increases slowly, undergoes a rapid increase at a characteristic pressure P_N , and tends to evolve through a broad hump for $P \geq P_N$. As shown in Fig. 6(b), the feature at P_N is absent for $T \gg T_N$, indicating that it is strictly associated with the low-temperature magnetism. By connecting P_N with the antiferromagnetic phase boundary from measurements at constant P , we infer that the rapid increase in $\rho(P)$ at P_N represents the magnetic phase boundary, which drops sharply to $T = 0$ over this T - P range. In order to search for superconductivity near this possible QPT, we measured electrical resistivity for $T > 300$ mK for $P = 1.2$ and 1.37 GPa. These measurements did not show any evidence for superconductivity.

V. DISCUSSION

From the measurements above, we construct a magnetic phase diagram [Fig. 7(a)]. For $P = 0$, χ , C , and ρ reveal an antiferromagnetic phase transition near $T_N \approx 110$ K. The values of T_N that we find from C and ρ are slightly smaller than those found from χ owing to differing conventions for defining T_N . We additionally find a subsequent feature in the ordered state, as evidenced by the reduction in $\chi(T)$ at T_1 . For increasing pressure, T_N is initially suppressed at a rate of -33 K/GPa. For $P \geq 0.89$ GPa, a second phase transition appears within the ordered state at T_2 which is also suppressed by P . While it is appealing to connect T_2 to the reduction of $\chi(T)$ at T_1 for $P = 0$, our measurements do not necessarily show that this is the case. In fact, our data suggest that the

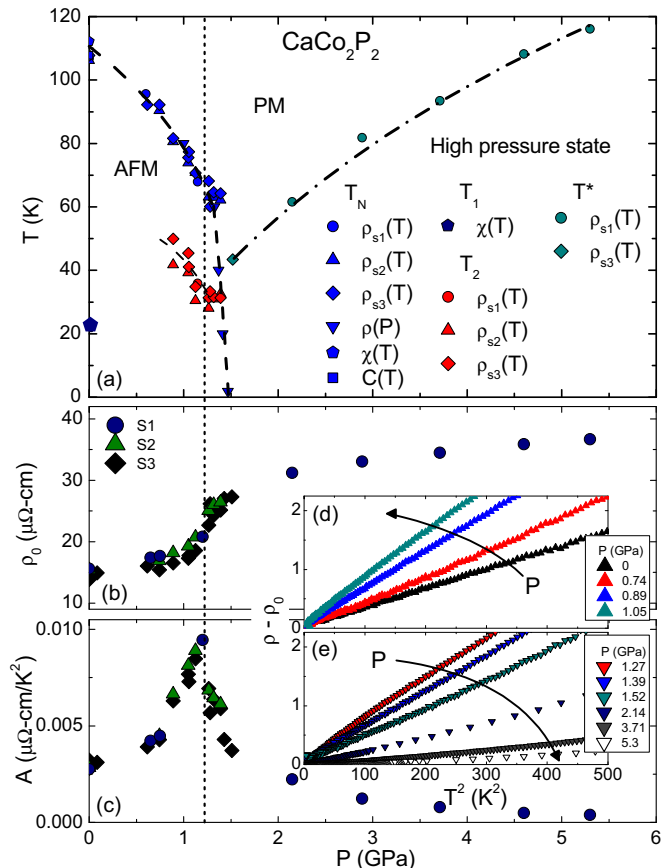


FIG. 7. (Color online) (a) Temperature T vs pressure P phase diagram for CaCo_2P_2 constructed from magnetic susceptibility χ , heat capacity C , and electrical resistivity ρ measurements. The phase boundary described by T_N separates the paramagnetic (PM) state for $T \geq T_N$ from the antiferromagnetically (AFM) ordered state for $T \leq T_N$. T_1 represents the T where the zero P magnetic susceptibility decreases abruptly below T_N , as described in the text. T_2 represents changes in low T electronic scattering for $T < T_N$ which appear as humps in $\partial\rho/\partial T$. T_N is suppressed to a putative quantum phase transition near $P_c = 1.4$ – 1.5 GPa. T^* is the broad hump in $\partial\rho/\partial T$ which appears for $P > P_c$. (b) The residual resistivity ρ_0 vs P taken from fits to $\rho(T)$, as described in the text. (c) Fermi-liquid coefficient of the electrical resistivity A taken from fits to $\rho(T)$. (d) $\rho - \rho_0$ vs T^2 for $P \leq 1.05$ GPa. (e) $\rho - \rho_0$ vs T^2 for $P \geq 1.27$ GPa.

broad hump that appears in $\partial\rho/\partial T$ for $P < 0.89$ GPa is more naturally connected to T_2 . Near $P_c = 1.4$ – 1.5 GPa, T_N and T_2 are suppressed abruptly to zero at a putative quantum phase transition, where the sharp phase boundary suggests that the transition may become first order. Upon destruction of the low P magnetic order at P_c , a broad feature appears at T^* which increases and broadens with increasing P . These results raise several unresolved questions that complicate our understanding of this material, including (1) the nature of the phase transition(s) near P_c and (2) the details of the high-pressure state. Below, we outline several scenarios for understanding the data and suggest measurements to resolve these issues.

Regarding question 1, we point out that phase diagrams with similarly sharp phase boundaries have been observed

for some quantum critical point systems, e.g., the correlated electron antiferromagnet CeRh_2Si_2 , which additionally shows unconventional superconductivity at the putative QCP [39]. A similarly sharp phase boundary is found at low temperatures for the d -electron antiferromagnet system $\text{Cr}_{1-x}\text{V}_x$, where detailed Hall-effect measurements reveal that the phase transition is second order in the vicinity of the QCP [14]. As such, it is not clear that a sharp phase boundary necessarily implies that the phase transition becomes first order. In order to resolve this issue, it will be useful to study the evolution of the magnetic order parameter under applied pressure, e.g., using neutron-scattering or NMR measurements.

It is also noteworthy that the phase diagram for CaCo_2P_2 shows similarities to some systems with ferromagnetic quantum phase transitions. For instance, the itinerant electron ferromagnet UGe_2 exhibits two phase transitions that are suppressed toward zero with P [40]. In this case, both phase transitions are first order near $T = 0$ [41], as is expected for a ferromagnetic phase (either due to coupling between fermionic modes and ferromagnetic critical fluctuations or magnetoelastic coupling) [42–44]. Given the observation of ferromagnetic correlations at zero pressure for $T > T_N$ in CaCo_2P_2 , it is not unreasonable to consider that ferromagnetism might emerge with P . It is also noteworthy that the closely related LaCo_2P_2 (where La is trivalent) orders ferromagnetically near $T_C = 160$ K, suggesting that electron doping might induce similar behavior in CaCo_2P_2 (where Ca is divalent) [45]. As such, it is tempting to draw connections to ferromagnetic phenomena. Again, neutron-scattering and NMR measurements will help to address this possibility. On the other hand, if the phase transition remains antiferromagnetic but becomes first order near the QPT, this might indicate that it is accompanied by an additional component, e.g., a structural phase transition. X-ray-diffraction measurements under applied pressure would clarify this point.

To address question 2, we first note that qualitatively similar features are observed in a variety of other systems without magnetic ordering: e.g., some A-15 compounds like Nb_3Sn and Nb_3Sb exhibit strong negative curvature and rapid saturation to nearly constant values of $\rho(T)$ with increasing T that is related to strong electron-phonon coupling [46]. However, since magnetism obviously plays a role in the low-pressure region of the phase diagram, it is appealing to look for a magnetic description of the high-pressure data. From this viewpoint, one possibility is that a spin-fluctuation regime appears for $P > P_c$. In this scenario, the temperature dependence of the electrical resistivity is attributed to the presence of a large feature in the density of states near the Fermi energy due to the d electrons. We also point out that other d -electron spin-fluctuation compounds [e.g., RCO_2 ($R = \text{Y, Lu, Sc}$) [47] exhibit behavior that is similar to what we observe in the high P region for CaCo_2P_2 : i.e., the broad shoulder in $\rho(T)$ that characterizes the spin-fluctuation temperature broadens and moves to higher T with increasing P . On the other hand, it is possible that T^* might instead be related to an extremely broad magnetic phase transition, yielding a phase diagram with a transformation from low-pressure antiferromagnetism to a high-pressure magnetic state, similar to what is seen as a function of x for $\text{Ba}(\text{Fe}_{1-x}\text{M}_x)\text{As}_2$ ($M = \text{Cr, Mn}$) and $\text{Ca}(\text{Co}_{1-x}\text{Ni}_x)_2\text{P}_2$ [32,48,49]. We are currently

pursuing NMR measurements under pressure to address this question.

Finally, in order to further investigate the ground-state behavior we consider the expression

$$\rho(T) = \rho_0 + AT^2, \quad (2)$$

where ρ_0 is the residual resistivity and A is the Fermi-liquid coefficient of the electrical resistivity. Plots of $\rho - \rho_0$ vs T^2 are shown in Figs. 7(d) and 7(e), where linear behavior is observed, indicating that Fermi-liquid-like behavior is present for all P . This analysis shows that (much like the finite T behavior) the residual resistivity ρ_0 increases rapidly with increasing pressure near P_c and tends to saturate for $P \geq P_c$ [Fig. 7(b)]. In addition, we find that, for $P \leq P_c$, A increases with increasing P and reaches a maximum near $P = 1.22$ GPa, which is slightly less than $P_c = 1.4\text{--}1.5$ GPa [see Fig. 7(c)]. Such a divergence in A is a common feature in most QCP materials and may indicate that, upon approaching the quantum phase transition, the critical fluctuations begin to diverge. However, if the phase transition becomes first order, then the critical fluctuations are expected to be cut off, consistent with the rapid drop in A before P_c . For $P \geq P_c$, A relaxes toward a small value at high P . We note that similar behavior for $A(P)$ is observed for spin-fluctuation compounds (e.g., RCO_2), where the decrease in A with P is attributed to weakening spin fluctuations with increasing pressure [47].

Since Fermi-liquid behavior persists throughout the entire phase diagram, it is of interest to consider the Kadowaki-Woods ratio $R_{\text{KW}} = A/\gamma^2$ [50]. For $P = 0$, $R_{\text{KW}} \approx 0.6 \times 10^{-5} \mu\Omega \text{ cm}(\text{K}\cdot\text{mol}/\text{mJ})^2$, in reasonably good agreement with the expectation for a d -electron Fermi liquid [51]. If we assume that this ratio is constant as a function of pressure, then it is possible to calculate the electronic coefficient of the specific heat γ where A is at a maximum. This calculation yields $\gamma \approx 40 \text{ mJ}/\text{mol}\cdot\text{K}^2$ at $P = 1.22$ GPa, which is moderately enhanced by comparison to the zero pressure value of $23 \text{ mJ}/\text{mol}\cdot\text{K}^2$. While the origin of this behavior is not clear, we point out that enhanced correlations are regularly observed in a variety of related transition-metal pnictides. For instance, optical spectroscopy measurements which compare the experimental kinetic energy and the kinetic energy from band theory support this point of view [52].

VI. CONCLUSIONS

In summary, experiments indicate that CaCo_2P_2 is a moderately correlated itinerant electron antiferromagnet with an ordering temperature near $T_N \approx 110$ K. In addition, we find evidence for ferromagnetic correlations in the paramagnetic state and an additional feature at $T_1 = 22$ K. Electrical resistivity measurements under applied pressure reveal that T_N is suppressed initially with increasing P at a rate of $-33 \text{ K}/\text{GPa}$. Near 0.89 GPa, a second phase transition appears in the electrical resistivity at $T_2 < T_N$. At $P_c \approx 1.4\text{--}1.5$ GPa, the phase transition(s) may become first order as they are suppressed abruptly toward zero. For $P > P_c$, $\rho(T)$ exhibits a broad shoulder which increases and broadens in T with increasing P . Taken together, these observations suggest that CaCo_2P_2 provides the unusual example of a magnetic

d -electron metal where a quantum phase transition may be accessed by a clean tuning parameter.

Nonetheless, several important questions remain to be addressed. For zero pressure, it will be useful to perform NMR and neutron-scattering measurements to determine the nature of the phase transition at T_1 . It is also important to uncover whether the phase transitions near P_c are first or second order, as this determines whether divergent fluctuations of the order parameter are permitted. If the phase transition is first order, then it will be interesting to understand how this happens: e.g., two possible scenarios are that the magnetically ordered state become ferromagnetic or there is an additional structural phase transition. Finally, the nature of the high-pressure state remains to be clarified.

In spite of the factors that complicate our understanding of this material, there nonetheless are several opportunities. Primary among these is the chance to study a quantum phase transition in a moderately correlated d -electron magnet using a clean tuning parameter. The similarities between CaCo_2P_2 and other d - and f -electron QPT materials, such as MnSi , ZrZn_2 , and UGe_2 , may provide direction for developing a unifying theory for the physics of such systems. Comparison to the

Fe-As high-temperature superconductors is also of interest. For instance, the lack of superconductivity in CaCo_2P_2 may give an important clue about what ingredients are necessary to provide a pairing mechanism for superconductivity in the Fe-As analogs.

ACKNOWLEDGMENTS

We are grateful for valuable discussions with J. M. Lawrence, C. D. Batista, H. Sakai, and T. Park. Work at Los Alamos National Laboratory was performed under the auspices of the U.S. Department of Energy (DOE), Office of Basic Energy Sciences, Division of Materials Sciences and Engineering. R. E. Baumbach acknowledges Presidential Early Career Awards for Scientists and Engineers funding from the U.S. DOE, Office of Basic Energy Sciences, Division of Material Science and Engineering and support from the Los Alamos Director's Postdoctoral Program. This work was performed, in part, at the Center for Integrated Nanotechnologies, a U.S. Department of Energy, Office of Basic Energy Sciences user facility.

-
- [1] G. R. Stewart, *Rev. Mod. Phys.* **73**, 797 (2001).
 [2] H. v. Löhneysen, A. Rosch, M. Vojta, and P. Wölfle, *Rev. Mod. Phys.* **79**, 1015 (2007).
 [3] C. Pfleiderer, *Rev. Mod. Phys.* **81**, 1551 (2009).
 [4] M. B. Maple, R. E. Baumbach, N. P. Butch, J. J. Hamlin, and M. Janoschek, *J. Low Temp. Phys.* **161**, 4 (2010).
 [5] J. Dai, Q. Si, J.-X. Zhu, and E. Abrahams, *Proc. Natl. Acad. Sci. USA* **106**, 4118 (2009).
 [6] N. P. Butch, K. Jin, K. Kirshenbaum, R. L. Greene, and J. P. Paglione, *Proc. Natl. Acad. Sci. USA* **109**, 8440 (2012).
 [7] C. Pfleiderer, G. J. McMullan, S. R. Julian, and G. G. Lonzarich, *Phys. Rev. B* **55**, 8330 (1997).
 [8] M. Janoschek, M. Garst, A. Bauer, P. Krautscheid, R. Georgii, P. Böni, and C. Pfleiderer, *Phys. Rev. B* **87**, 134407 (2013).
 [9] C. Pfleiderer, S. R. Julian, and G. G. Lonzarich, *Nature (London)* **414**, 427 (2001).
 [10] M. Uhlarz, C. Pfleiderer, and S. M. Hayden, *Phys. Rev. Lett.* **93**, 256404 (2004).
 [11] R. P. Smith, M. Sutherland, G. G. Lonzarich, S. S. Saxena, N. Kimura, S. Takashima, M. Nohara, and H. Takagi, *Nature (London)* **455**, 1220 (2008).
 [12] D. A. Sokolov, M. C. Aronson, W. Gannon, and Z. Fisk, *Phys. Rev. Lett.* **96**, 116404 (2006).
 [13] M. Sato, *J. Phys. Soc. Jpn.* **39**, 98 (1975).
 [14] M. Lee, A. Husmann, T. F. Rosenbaum, and G. Aeppli, *Phys. Rev. Lett.* **92**, 187201 (2004).
 [15] G. Just and P. Pauffer, *J. Alloys Compd.* **232**, 1 (1996).
 [16] F. M. Grosche, S. R. Julian, N. D. Mathur, and G. G. Lonzarich, *Physica B* **223-224**, 50 (1996).
 [17] J. Custers, P. Gegenwart, H. Wilhelm, K. Neumaier, Y. Tokiwa, O. Trovarelli, C. Geibel, F. Steglich, C. Pepin, and P. Coleman, *Nature (London)* **424**, 524 (2003).
 [18] D. C. Johnston, *Adv. Phys.* **59**, 803 (2010).
 [19] S. A. Jia, A. J. Williams, P. W. Stephens, and R. J. Cava, *Phys. Rev. B* **80**, 165107 (2009).
 [20] F. Ronning, E. D. Bauer, T. Park, S. H. Baek, H. Sakai, and J. D. Thompson, *Phys. Rev. B* **79**, 134507 (2009).
 [21] N. Berry, C. Capan, G. Seyfarth, A. D. Bianchi, J. Ziller, and Z. Fisk, *Phys. Rev. B* **79**, 180502 (2009).
 [22] J. J. Hamlin, R. E. Baumbach, D. A. Zocco, T. A. Sayles, and M. B. Maple, *J. Phys.: Condens. Matter* **20**, 365220 (2008).
 [23] R. E. Baumbach, J. J. Hamlin, L. Shu, D. A. Zocco, N. M. Crisosto, and M. B. Maple, *New J. Phys.* **11**, 025018 (2009).
 [24] R. E. Baumbach, J. J. Hamlin, P.-C. Ho, I. K. Lum, and M. B. Maple, *Phys. Rev. B* **85**, 104526 (2012).
 [25] M. Reehuis and W. Jeitschko, *J. Phys. Chem. Solids* **51**, 961 (1990).
 [26] R. Hoffman and C. Zheng, *J. Phys. Chem.* **89**, 4175 (1985).
 [27] J. G. Analytis, C. M. J. Andrew, A. I. Coldea, A. McCollam, J.-H. Chu, R. D. McDonald, I. R. Fisher, and A. Carrington, *Phys. Rev. Lett.* **103**, 076401 (2009).
 [28] A. I. Coldea, C. M. J. Andrew, J. G. Analytis, R. D. McDonald, A. F. Bangura, J. H. Chu, I. R. Fisher, and A. Carrington, *Phys. Rev. Lett.* **103**, 026404 (2009).
 [29] M. Reehuis, W. Jeitschko, G. Kotzyba, B. Zimmer, and X. Hu, *J. Alloys Compd.* **266**, 54 (1998).
 [30] E. Gustenau, P. Herzig, and A. Neckel, *J. Alloys Compd.* **262-263**, 516 (1997).
 [31] I. B. Shameem Banu, M. Rajagopalan, M. Yousuf, and P. Shenbagaraman, *J. Alloys Compd.* **288**, 88 (1999).
 [32] S. Jia, S. Chi, J. W. Lynn, and R. J. Cava, *Phys. Rev. B* **81**, 214446 (2010).
 [33] L. G. Khvostantsev, V. N. Slesarev, and V. V. Brazhkin, *High Press. Res.* **24**, 371 (2004).
 [34] A. E. Petrova, V. A. Sidorov, and S. M. Stishov, *Physica B* **359-361**, 1463 (2005).
 [35] P. Payet Burin, C. Pfleiderer, *Rev. Sci. Instrum.* **67**, 4023 (1996).

- [36] P. Blaha *et al.*, in *An Augmented Plane Wave + Local Orbitals Program for Calculating Crystal Properties*, edited by K. Schwartz (Vienna University of Technology, Vienna, 2001).
- [37] J. P. Perdew, K. Burke, and M. Ernzerhof, *Phys. Rev. Lett.* **77**, 3865 (1996).
- [38] E. Colombier, S. L. Bud'ko, N. Ni, and P. C. Canfield, *Phys. Rev. B* **79**, 224518 (2009).
- [39] R. Movshovich, T. Graf, D. Mandrus, M. F. Hundley, J. D. Thompson, R. A. Fisher, N. E. Phillips, and J. L. Smith, *Physica B* **223-224**, 126 (1996).
- [40] N. Tateiwa, T. C. Kobayashi, K. Hanazono, K. Amaya, Y. Haga, R. Settai, and Y. Onuki, *J. Phys.: Condens. Matter* **13**, L17 (2001).
- [41] C. Pfleiderer and A. D. Huxley, *Phys. Rev. Lett.* **89**, 147005 (2002).
- [42] D. Belitz, T. R. Kirkpatrick, and T. Vojta, *Phys. Rev. Lett.* **82**, 4707 (1999).
- [43] V. P. Mineev, *Comptes Rendus Physique* **12**, 567 (2011).
- [44] M. Sutherland, R. P. Smith, N. Marcano, Y. Zou, S. E. Rowley, F. M. Grosche, N. Kimura, S. M. Hayden, S. Takashima, M. Nohara, and H. Takagi, *Phys. Rev. B* **85**, 035118 (2012).
- [45] M. Reehuis, C. Ritter, R. Ballou, and W. Jeitschko, *J. Magn. Magn. Mater.* **138**, 85 (1994).
- [46] Z. Fisk and G. W. Webb, *Phys. Rev. Lett.* **36**, 1084 (1976).
- [47] R. Hauser, E. Bauer, and E. Gratz, *Phys. Rev. B* **57**, 2904 (1998).
- [48] K. Marty, A. D. Christianson, C. H. Wang, M. Matsuda, H. Cao, L. H. VanBebber, J. L. Zarestky, D. J. Singh, A. S. Sefat, and M. D. Lumsden, *Phys. Rev. B* **83**, 060509(R) (2011).
- [49] A. Thaler, H. Hodovanets, M. S. Torikachvili, S. Ran, A. Kracher, W. Straszheim, J. Q. Yan, E. Mun, and P. C. Canfield, *Phys. Rev. B* **84**, 144528 (2011).
- [50] K. Kadowaki and S. B. Woods, *Solid State Commun.* **58**, 507 (1986).
- [51] A. C. Jacko, J. O. Fjaerestad, and B. J. Powell, *Nature Phys.* **5**, 422 (2009).
- [52] M. M. Qazilbash, J. J. Hamlin, R. E. Baumbach, L. Zhang, D. J. Singh, M. B. Maple, and D. N. Basov, *Nature Phys.* **5**, 647 (2009).